

Density Tunable Graphene Aerogels Using a Sacrificial Polycyclic Aromatic Hydrocarbon

Sally Turner, Hu Long, Brian Shevitski, Thang Pham, Maydelle Lorenzo, Ellis Kennedy, Shaul Aloni, Marcus Worsley, and Alex Zettl*

We demonstrate a new strategy to tune the density of graphene aerogels. This facile method is capable of producing graphene aerogels over a wide density range without compromising the morphology or quality of the material. Perylenetetracarboxylic acid dianhydride serves as a sacrificial filler material that can be thermally decomposed to yield a graphene aerogel with tunable density.

1. Introduction

Since Novoselov and Geim's seminal work on the isolation of graphene and exploration of its extraordinary properties,^[1] interest in the material has exploded. The single layer of sp² bonded carbon has excellent electrical, thermal and mechanical properties, as well as excellent chemical and thermal stability. For this reason, it has been proposed in many applications including electronics,

composite materials, as well as energy harvesting and storage.^[2–5]

In order to adapt nanoscale graphene for these macroscale applications, an ability to synthesize material that incorporates substantial quantities of graphene can be crucial. Graphene aerogels are a class of graphitic materials containing cross-linked graphene in a three dimensional structure. They are low density, high surface area, porous materials that can be synthesized on

the gram scale. The properties of the 2D graphene building blocks of 3D graphene aerogels are largely retained. Graphene aerogels have high electrical conductivities, excellent mechanical properties, and favorable chemical and thermal stability.^[6,25–27] Due to these properties, in conjunction with surface areas approaching the theoretical limit of graphene, mesoporous and macroporous structures, and ultra-low densities, graphene aerogels have already been widely incorporated into a variety of applications including supercapacitor and battery electrodes, hydrogen storage, catalysis, chemical sensing, and water treatment.^[7–12] Many scalable syntheses of graphene aerogels have been developed that can incorporate grams of graphene material into one single, multifunctional structure,^[6,13–15] and a large degree of progress has been made in controlling and optimizing the crystallinity of graphene aerogels.^[16] However, there is still a need for synthetic control of their macroscopic properties. Aerogel density, porosity, surface area and mechanical properties are essential for material performance, but individual applications require specific and well-defined properties. For example, control of meso and macropore architectures in graphene aerogels used for supercapacitor electrodes allows multidimensional electron transport resulting in increased performance.^[17] Furthermore, control over elasticity of graphene aerogels opens potential applications for energy dampening or in biology.^[13]

Tuning the density of graphene aerogels can be a critical step towards the design of a truly optimized material. Moreover, many physical properties scale with density including electrical and thermal conductivity. Thus, the ability to tune the density of graphene aerogels could open up the opportunity to have control over electrical and thermal properties.

Tunable densities and mechanical properties of carbon aerogels synthesized using organic sol–gel chemistry of resorcinol and formaldehyde have been extensively documented.^[18] However, to date, there are few examples of tuning properties of graphene aerogels by altering gelation conditions.^[21–24]

In this work, we present a facile strategy toward tuning the density of graphene aerogels using perylenetetracarboxylic acid

S. Turner, Dr. H. Long, B. Shevitski, T. Pham, M. Lorenzo, E. Kennedy, Prof. A. Zettl
Department of Physics, University of California at Berkeley, Berkeley, CA 94720, USA
E-mail: azettl@berkeley.edu

S. Turner, M. Lorenzo
Department of Chemistry, University of California at Berkeley, Berkeley, CA 94720, USA

S. Turner, Dr. H. Long, B. Shevitski, T. Pham, Prof. A. Zettl
Kavli Energy NanoScience Institute at the University of California, Berkeley and the Lawrence Berkeley National Laboratory, Berkeley, CA 94720, USA

B. Shevitski, Dr. S. Aloni
The Molecular Foundry, Lawrence Berkeley National Laboratory, Berkeley, CA 94720, USA

T. Pham, E. Kennedy
Department of Materials Science and Engineering, University of California at Berkeley, Berkeley, CA 94720, USA

Dr. M. Worsley
Physical and Life Sciences Directorate, Lawrence Livermore National Laboratory, Livermore, CA 94550, USA

Prof. A. Zettl
Materials Sciences Division, Lawrence Berkeley National Laboratory, Berkeley, CA 94720, USA

DOI: 10.1002/pssb.201700203

(PTCDA) as a sacrificial molecule. To the best of our knowledge, this is the first process that can tune an aerogel to both lower and higher density in one single method, while maintaining the porous structure of the material.

2. Experimental

Graphene aerogels are synthesized by making a 20 mg mL⁻¹ solution of graphene oxide (GO) (CheapTubes) in water. The amount of PTCDA (Sigma–Aldrich) for the desired PTCDA:GO ratio is added into this suspension. All samples contain the same GO content, while the PTCDA amount is varied. 16 vol.% of ammonium hydroxide is added and heated to 80 °C for 3 days. Samples are exchanged into acetone and dried using supercritical CO₂ resulting in PTCDA/GO aerogels. Aerogels are thermally reduced at 1050 °C in an Ar atmosphere. Samples reduced at 2000 °C are first fired to 1050 °C in Ar and subsequently fired at 2000 °C in He.

Densities are measured using the mass and physical dimensions of the samples. Scanning Electron Microscopy (SEM) is performed on an FEI Sirion microscope with 5 kV accelerating voltage. Transmission Electron Microscopy (TEM) is performed on a JEOL 2010 microscope under 80 kV accelerating voltage. Raman Spectroscopy is completed on a Renishaw inVia spectrometer with 514 nm excitation laser. XRD is taken on a Bruker AXS D8 Discover GADDS X-Ray Diffractometer with CoK α (1.79 Å) source. Fourier Transform Infrared Spectroscopy (FTIR) was performed on a Nicolet 6700 instrument with the attenuated total reflectance accessory and diamond plate.

3. Results

Graphene aerogels are synthesized using a base catalyzed synthesis. Over the course of this reaction, functional groups on graphene oxide chemically crosslink and deoxygenate to form a hydrogel.^[15,19] During this process, hydrogels undergo shrinkage and densification. In order to tune the density of graphene aerogels, control over this volume shrinkage is targeted. A polycyclic aromatic hydrocarbon (PAH) is added into the graphene aerogel to reduce the volume shrinkage during gelation. It is important that the PAH be soluble in water, not participate in the gelation reaction, and be thermally decomposed after synthesis. PTCDA, a common red dye and n-type semiconductor used in optoelectronics, is suspendable in water, does not interfere with gelation, and can be decomposed at 450 °C.

As shown in **Figure 1a**, PTCDA is added into the GO suspension and undergoes gelation using an ammonium hydroxide catalyst. GO content is kept constant in all samples and PTCDA content is altered to prepare aerogels of specific PTCDA:GO ratios. After gelation, the graphene oxide hydrogels are dried using supercritical CO₂ and GO/PTCDA aerogels are thermally treated to decompose the PTCDA and reduce GO, yielding graphene aerogels with controlled density. Due to the optical properties of the PTCDA, the GO/PTCDA aerogels have a red color (**Figure 1c**). After reduction, they turn the characteristic black color of graphene aerogels. The series of aerogels varying from no PTCDA to 15 times the mass of PTCDA to GO is shown in **Figure 1d**. It is clear

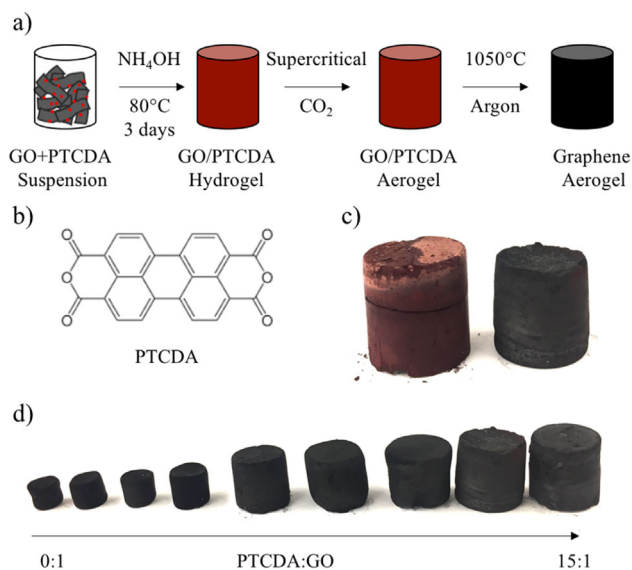


Figure 1. (a) Schematic of density tunable graphene aerogel synthesis. (b) Structure of PTCDA used as sacrificial PAH. (c) Samples containing 10:1 PTCDA:GO before thermal reduction and decomposition (left) and after heating to 1050 °C (right). (d) Photograph of series of graphene aerogels with increasing PTCDA content.

that the degree of aerogel shrinkage during gelation is significantly reduced with increased PTCDA content.

The morphologies of PTCDA/GO aerogels and graphene aerogels are characterized using SEM and TEM. As shown in **Figure 2a**, fibers are formed within the graphene oxide aerogel that are not present in the control. They are present in the 1:1 (PTCDA:GO) graphene oxide aerogels and are the dominant species in the 15:1 material (**Figure 2c**). These fibers are the result of a reaction between the PTCDA and the ammonium hydroxide catalyst and graphene oxide does not play a role in their formation (**Figure S1**, see Supporting Information). It is known that PAHs can self-assemble into one dimensional nanostructures due to pi-pi interactions between aromatic rings.^[20] Thus, the formation of nanofibers is not unexpected and they play a key role in preventing shrinkage during gelation. Nanofibers visible under SEM are 100–200 nm in diameter and are not found under TEM (likely due to the pi stacking not withstanding sonication during sample preparation). Smaller nanofibers around 10 nm assembled directly on GO are observed under TEM (**Figure 2e**). Fibers of all sizes are noticeably missing after thermal reduction at 1050 °C (**Figure 2b,d,f**). Thermogravimetric analysis (not shown) indicates that the fibers decompose at 450 °C and no longer remain at 1050 °C. After decomposition of nanofibers, the graphene aerogel has a porous structure and wrinkled graphene sheets indicative of a typical graphene aerogel (**Figure 2b,d,f**). This indicates that PTCDA does not interfere with gelation in the formation of a hydrogel or change the aerogel morphology.

Gelation is performed in a vial resulting in graphene aerogel cylinders and the shrinkage during gelation is calculated by taking the fraction of the graphene aerogel diameter to the diameter of the gelation vial. The percent shrinkage during gelation as a function of PTCDA:GO shows two clear regimes

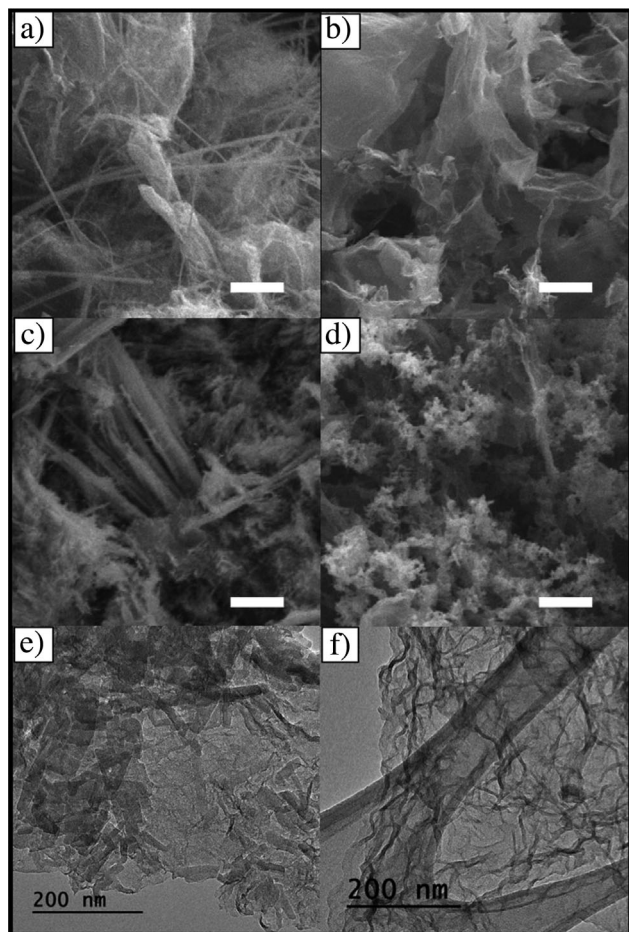


Figure 2. (a–b) SEM images of aerogels with 1:1 before and after thermal reduction, respectively. (c–d) 15:1 PTCDA:GO before thermal reduction and after, respectively. Scale bars in a–d are 2 μm . (e) TEM image of 1:1 PTCDA:GO aerogels before reduction and (f) after thermal reduction and decomposition of nanofibers.

(Figure 3a). At PTCDA:GO less than 1, there is a decreasing shrinkage with increased PTCDA, meaning that the aerogel volume is larger. However, a minimum shrinkage of around 10% is reached when PTCDA:GO is 2.5 and additional PTCDA does not affect shrinkage during gelation. A control graphene aerogel shrinks around 50% during gelation, so an aerogel with the same mass and 10% shrinkage would have a density 80% smaller than the control.

The other contributor to aerogel density is the mass. Incomplete decomposition of nanofibers can affect the density and even lead to densities higher than the control without destroying the porous structure. If decomposition of PTCDA were complete, all aerogels would have the same mass due to the normalized GO content across samples. However, a fraction of the mass from PTCDA is retained inside the aerogel, resulting in increasing mass with increased PTCDA content (Figure 3a). The additional mass has likely turned into amorphous carbon inside the aerogel or is partially incorporated into the graphene. However, at higher PTCDA content, some nanofibers are still observed under SEM. Partial decomposition to amorphous

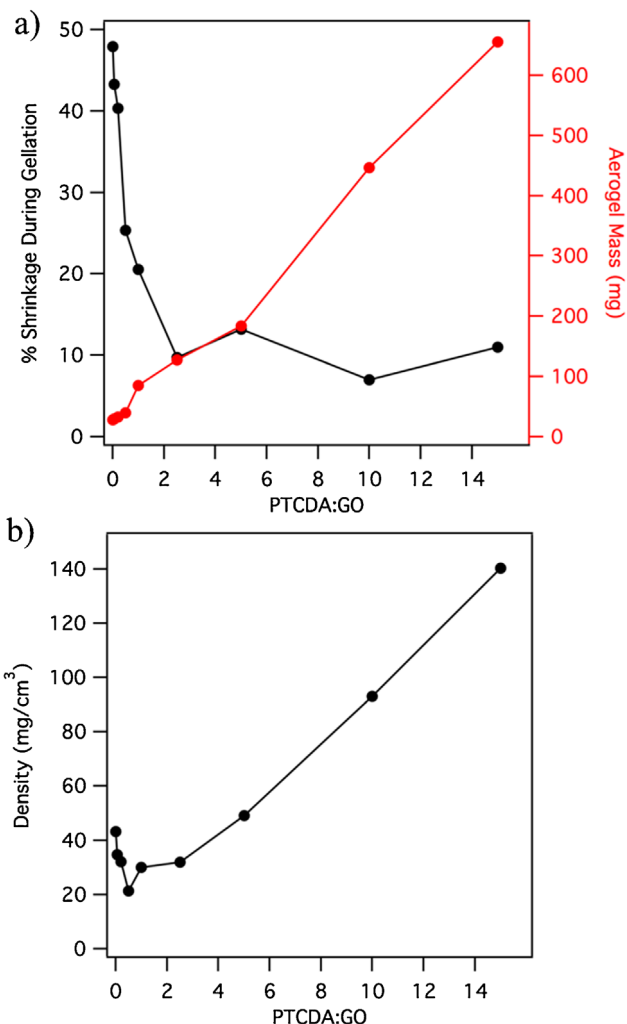


Figure 3. (a) Shrinkage of graphene aerogels with increasing PTCDA content during gelation on left axis, with 0:1 aerogel being the control. Mass of aerogels with increasing PTCDA content on right axis. (b) Density of graphene aerogels showing a minimum at 0.5:1 PTCDA:GO and increasing density with increased PTCDA between 1:1 and 15:1. All aerogels have been heat treated at 1050 $^{\circ}\text{C}$.

carbon or incorporation into graphene enables the synthesis of higher density aerogels.

The mass of aerogels and the volume shrinkage with increasing PTCDA content are competing terms. At low PTCDA content, the increased volume dominates compared to the small increase in mass, resulting in decreased aerogel density (Figure 3b). A maximum density reduction of 50% is achieved when PTCDA:GO is 1:2. PTCDA:GO ratios larger than 1:2 result in a higher density due to both the increasing mass and having reached the minimum volume shrinkage. Drastic density increases are observed at large PTCDA content and a three fold densification is achieved at 15:1 (PTCDA:GO). Xerogels, hydrogels dried under ambient conditions, have completely collapsed pore structures due to solvent evaporation with surface tension. This typically leads to densities 10 times that of the control.^[21] Thus a threefold

densification while retaining a porous material is a significant achievement.

Further characterization of the material is performed to study the composition of the graphene aerogels. Before thermal reduction and decomposition of the nanofibers, the Raman spectrum is dominated by the modes of the PAH nanofibers and the characteristic graphitic peaks from the graphene oxide are not visible (Figure 4a). It is noted that the nanofibers have a large background signal at large wavenumbers. After thermal reduction, the signature Raman spectrum of graphene is obtained (Figure 4a and b). The graphene G peak due to the E_{2g} in plane phonon is observed at 1588 cm^{-1} , and the D peak which arises due to defects or scattering sites in the material is found at 1355 cm^{-1} . The 2D peak at 2705 cm^{-1} is a 2 phonon mode indicative of a graphitic material.

With increasing PTCDA content, the material exhibits an increase in the height and width of the D peak. Typically, the ratio of the intensity of the D peak to the G peak is used to assess the quality of graphene. Peaks from residual nanofibers would overlap with the D and G peaks of the graphene aerogels, so this analysis is not valid. The increased width of the D peak is

attributed to the presence of the overlapping peaks. While nanofibers have a strong background signal at large Raman shifts, no strong background signal is present after thermal reduction. This, in combination with the fact that overlapping peaks are so small that the characteristic graphene spectrum is recovered, indicates that some nanofibers still exist, but only a small fraction. Thus, the predominant species in the reduced aerogel is graphene.

X-ray diffraction is performed to evaluate the crystal structure of the graphene aerogels (Figure 4d). The diffractogram shows two peaks in graphene aerogels at 29° corresponding to the (002) plane of graphene ($d = 3.47\text{ \AA}$). Additionally, there is a weak peak at 50° due to the (100) and (101) planes.^[16,28] The crystalline nanofibers contain many diffraction peaks, some of which are overlapping with the (002) peak in graphene aerogels. With increased PTCDA content, the 29° peak becomes more prominent. While some increase in the (002) peak could be attributed to underlying peaks from the nanofibers, it is also likely caused by the increased abundance of this plane due to incorporation of additional mass into the graphene. Additionally, there is no direct observation of any nanofiber peaks even at

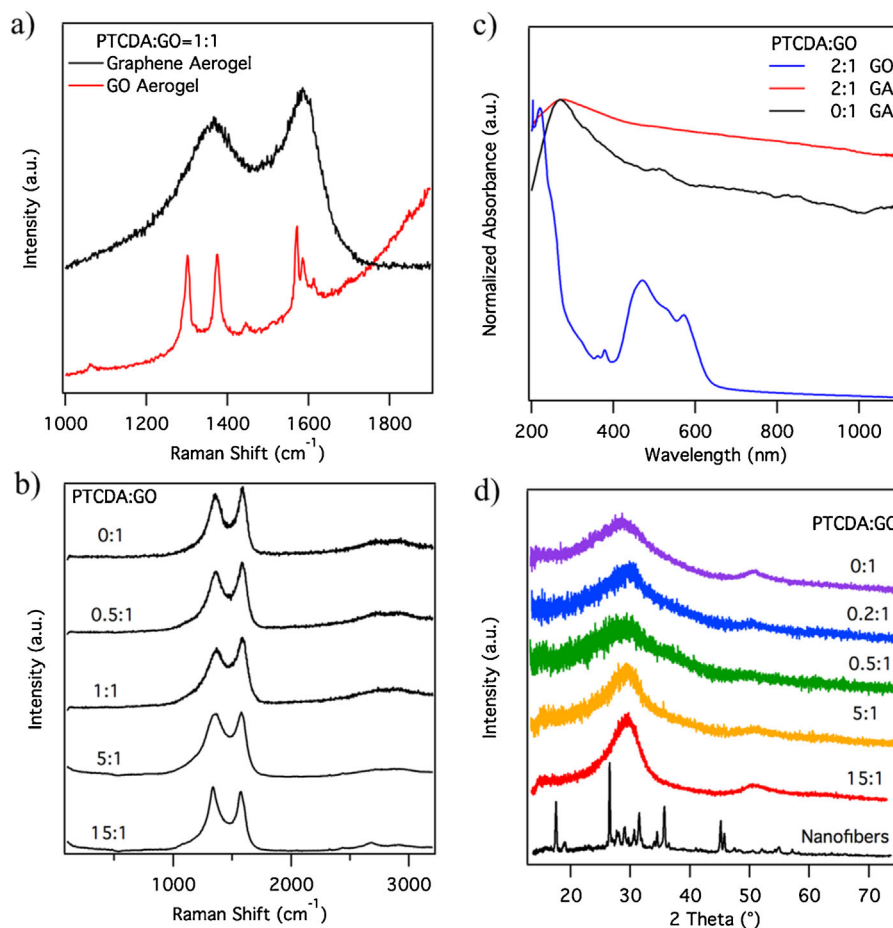


Figure 4. (a) Raman spectrum of 1:1 (PTCDA:GO) aerogels before and after thermal reduction. (b) Raman spectra of thermally reduced graphene aerogels with increasing PTCDA content. (c) UV-Vis absorbance spectra of 2:1 (PTCDA:GO) aerogel before and after thermal reduction compared with control GA. (d) XRD patterns of PAH nanofibers and graphene aerogels with increasing PTCDA content.

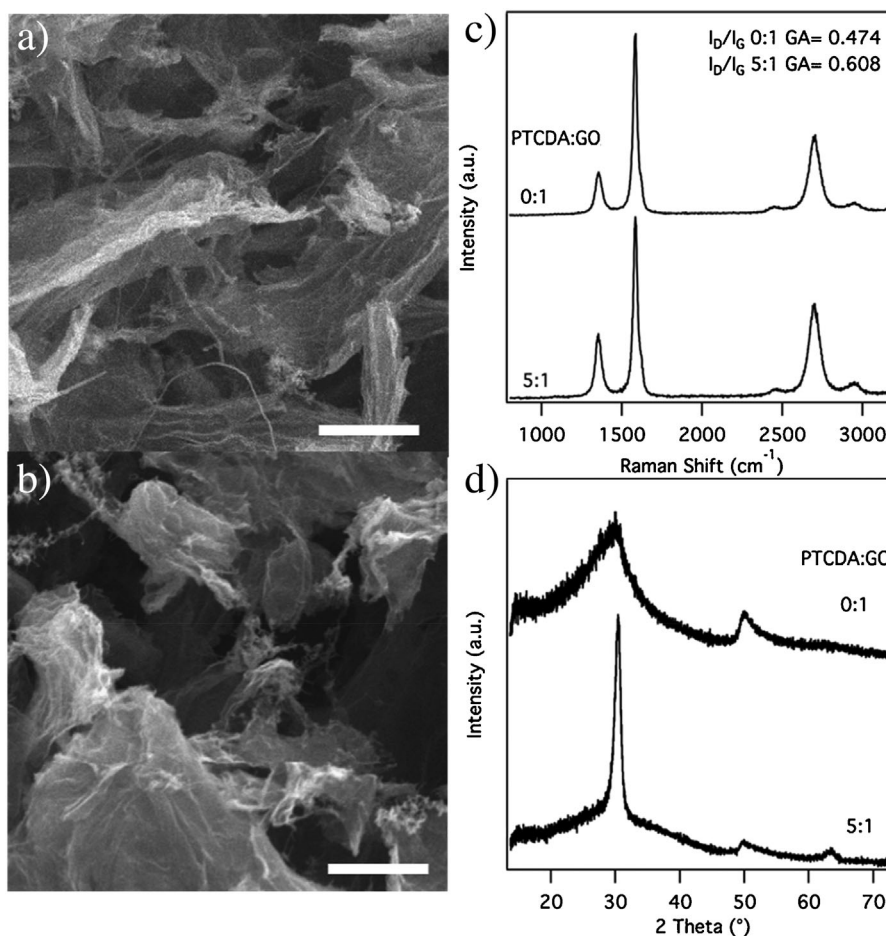


Figure 5. (a–b) SEM image of 5:1 (PTCDA:GO) aerogel treated at 1050 and 2000 °C, respectively. Scales bar are 2 μm. (c) Raman spectra of control graphene aerogel and 5:1 (PTCDA:GO) aerogel both treated at 2000 °C and (d) XRD patterns of 2000 °C control and 5:1 graphene aerogels.

PTCDA:GO ratio of 15:1. This further supports that graphene is the dominant structure in the reduced product, but some undecomposed nanofibers likely remain.

Using UV–Vis absorbance spectroscopy, the 2:1 PTCDA:GO aerogel spectrum is dominated by the absorbance of the PAH nanofibers at 220 nm and 400–600 nm (Figure 4c). The UV–Vis absorption spectra of both control graphene aerogels and 2:1 (PTCDA:GO) graphene aerogels show a strong peak at 275 nm due to π to π^* transitions indicative of the π conjugation in the graphene systems. Absorbance across the entire UV-Visible spectrum is decreased upon graphitization, in agreement with reports in the literature.^[19] Peaks present in the 2:1 (PTCDA:GO) sample disappear after treatment at 1050 °C, confirming that most PAH nanofibers are decomposed after thermal treatment.

FTIR studies were completed to further study the presence of nanofibers after thermal reduction. Graphene materials show no distinct FTIR peaks, while PAH nanofibers have a strong IR signal. With increasing PTCDA content, no features from nanofibers emerge in reduced aerogels (Figure S2a). Furthermore, the peaks due to PAH nanofibers in 2:1 (PTCDA:GO) aerogels before reduction disappear after heating to 1050 °C and the IR spectra of reduced aerogels are similar to the control

(Figure S2b,c) further indicating that graphene is the predominant species in the reduced aerogels.

To eliminate the potential interference from remaining nanofibers or amorphous carbon, an aerogel with PTCDA:GO of 5:1 is thermally treated to 2000 °C. At this temperature no amorphous carbon or nanofibers should remain and additional mass would be lost or incorporated into the graphene lattice. The aerogel mass decreases 3% after treatment indicating that additional mass is likely incorporated into the graphene.

After treatment at 2000 °C, the graphene aerogel morphology is maintained and nanofibers that were present in the 5:1 (PTCDA:GO) aerogel fired at 1050 °C are no longer present (Figure 5a,b).

Treatment at such a high temperature increases the crystallinity of the graphene,^[16] which is apparent in the Raman spectrum (Figure 5c). The D and G peaks are narrower and the 2D peak becomes more prominent. There are no peaks from the nanofibers and no increase in the width of the D peak, indicating complete decomposition of the nanofibers. The average D to G ratio of the 5:1 (PTCDA:GO) graphene aerogel is 0.608 and the control is 0.474. Incorporation of the PAH into graphene would result in an increased D peak due to additional grain boundaries, scattering sites

and overall disorder in the graphene. Thus the increased ratio supports the incorporation of the PAH into the graphene. The XRD diffractogram shows remarkable changes compared to the control aerogel thermally treated to 2000 °C (Figure 5d). The (002) peak increases in intensity and has a decreased width, indicating enhanced stacking and less curvature of graphene sheets. There is a decrease in the intensity of the (100) and (101) peaks also indicating more stacking of graphene. Lastly, a peak at 64° is present, corresponding to the (004) plane and is also due to the increasing layering in the material. Enhanced stacking of graphene sheets supports the incorporation of PAH nanofibers into the graphene lattice and no peaks from the PAH nanofibers are present.

Thus the entire series of aerogels with increasing PTCDA:GO can be fired at 2000 °C to improve the crystallinity of the material and incorporate the PAH into the graphene without compromising the density.

4. Conclusion

A facile method to tune the density of graphene aerogels to both lower and higher densities is presented, using PTCDA incorporation. After thermal reduction, additional carbon and a small amount of PAH nanofibers remain, but a higher temperature firing can eliminate the presence of these. By also incorporating changes in GO concentration in the suspension, we suspect a wider density range could be achieved.

Supporting Information

Supporting Information is available from the Wiley Online Library or from the author.

Acknowledgements

This work was supported in part by the Director, Office of Science, Office of Basic Energy Sciences, Materials Sciences, and Engineering Division, of the US Department of Energy under Contract No. DE-AC02-05-CH11231, within the sp²-Bonded Materials Program (KC2207) (TEM and SEM characterization), and within the Molecular Foundry (additional TEM characterization); by the Air Force Office of Scientific Research under Award No. FA9550-14-1-0323 (synthesis); and at LLNL under the auspices of the US Department of Energy under contract No. DE-AC52-07NA27344 (supplementary synthesis and structural characterization). ST acknowledges support from an NSF GRFP Fellowship.

Conflict of Interest

The authors declare no conflict of interest.

Keywords

aerogels, graphene, hydrocarbons, surfaces

Received: May 3, 2017

Revised: June 26, 2017

Published online:

References

- [1] A. K. Geim, K. S. Novoselov, *Nat. Mater.* **2007**, *6*, 183.
- [2] Y. M. Lin, C. Dimitrakopoulos, K. Jenkins, D. B. Farmer, H. Y. Chiu, A. Grill, P. Avouris, *Science* **2010**, *327*, 80.
- [3] S. Stankovich, D. A. Dikin, G. H. B. Dommett, K. M. Kohlaas, E. J. Zimney, E. A. Stach, S. T. Nguyen, R. S. Ruoff, *Nature* **2006**, *442*, 282.
- [4] X. Wang, L. Zhi, K. Mu, *Nano Lett.* **2008**, *8*, 323.
- [5] R. Raccichini, A. Varzi, S. Passerini, B. Scrosati, *Nature Mater.* **2015**, *14*, 271.
- [6] M. A. Worsley, P. Pauzauski, T. Olson, J. Biener, J. Satcher, T. Baumann, *J. Am. Chem. Soc.* **2010**, *132*, 14067.
- [7] S. Ye, J. Feng, P. Wu, *ACS Appl. Mater. Interfaces* **2013**, *5*, 7122.
- [8] B. Qiu, M. Xing, J. Zhang, *J. Am. Chem. Soc.* **2014**, *136*, 582.
- [9] K. Houria, T. Baumann, J. Satcher, A. Saulnier, C. Ahn, *Chem. Mater.* **2006**, *18*, 6085.
- [10] Y. Zhao, C. Hu, Y. Hu, H. Cheng, G. Shi, L. Qu, *Angew. Chem.* **2012**, *124*, 11533.
- [11] A. Harley-Trochimczyk, J. Chang, J. Zhou, Q. Zhou, J. Dong, T. Pham, M. Worsley, R. Maboudian, A. Zettl, W. Mickelson, *Sens. Actuators B, Chem.* **2015**, *206*, 399.
- [12] Z. Sui, Q. Meng, X. Zhang, R. Ma, B. Cao, *J. Mater. Chem.* **2012**, *22*, 8767.
- [13] H. Hu, Z. Zhao, W. Wan, Y. Gogotsi, J. Qiu, *Adv. Mater.* **2013**, *25*, 2219.
- [14] J. Biener, S. Dasgupta, L. Shao, D. Wang, M. Worsley, A. Wittstock, J. Lee, M. Biener, C. Orme, S. Kucheyev, B. Wood, T. Willey, A. Hamza, J. Weisenmuller, H. Hahn, T. Baumann, *Adv. Mater.* **2012**, *24*, 5083.
- [15] M. A. Worsley, S. Kucheyev, H. Mason, M. Merrill, B. Mayer, J. Lewicki, C. Valdez, M. Suss, M. Stadermann, P. Pauzauskie, J. Satcher, J. Biener, T. Bauman, *Chem. Commun.* **2012**, *48*, 8428.
- [16] M. A. Worsley, T. Pham, A. Yan, S. Shin, J. Lee, *J. Am. Chem. Soc.* **2014**, *8*, 11013.
- [17] S. M. Jung, D. L. Mafra, C. T. Lin, H. Jung, J. Kong, *Nanoscale* **2015**, *7*, 4386.
- [18] A. ElKhatat, S. Al-Muhtaseb, *Adv. Mater.* **2011**, *23*, 2887.
- [19] A. Goldstein, W. Mickelson, A. Machness, G. Lee, M. Worsley, L. Woo, A. Zettl, *J. Phys. Chem. C* **2014**, *118*, 28855.
- [20] L. Zang, Y. Che, J. Moore, *Acc. Chem. Res.* **2008**, *41*, 1596.
- [21] M. Worsley, S. Charnvanichborikarn, E. Montalvo, S. Shin, *Adv. Funct. Mater.* **2014**, *24*, 4259.
- [22] M. A. Worsley, T. Olson, J. Lee, T. Willey, M. Nielsen, S. K. Roberts, P. Pauzauskie, J. Biener, J. Satcher, T. Baumann, *J. Phys. Chem. Lett.* **2011**, *2*, 921.
- [23] Y. Xu, K. Sheng, C. Li, G. Shi, *ACS Nano* **2010**, *4*, 4324.
- [24] Z. Han, Z. Tang, S. Shen, B. Zhao, G. Zheng, J. Yang, *Sci. Rep.* **2014**, *4*, 5025.
- [25] G. Li, X. Zhang, J. Wang, J. Fang, *J. Mater. Chem. A* **2016**, *43*, 17042.
- [26] H. Huang, P. Chen, X. Zhang, Y. Lu, W. Zhan, *Small* **2013**, *9*, 1397.
- [27] X. Zhang, Z. Sui, B. Xu, S. Yue, Y. Luo, W. Zhan, B. Liu, M. Lima, M. Haque, Y. Gartstein, M. Zhang, A. Zakhidov, R. Baughman, *J. Mater. Chem.* **2011**, *21*, 6494.
- [28] Z. Li, C. Lu, Z. Xia, Y. Zhou, Z. Luo, *Carbon* **2007**, *45*, 1686.